Development/Plasticity/Repair

Cerebellar GABA Change during Visuomotor Adaptation Relates to Adaptation Performance and Cerebellar Network Connectivity: A Magnetic Resonance Spectroscopic Imaging Study

Caroline Nettekoven,[1,2,3,4] Leah Mitchell,[1] William T. Clarke,[1,3] Uzay Emir,[5] Jon Campbell,[1] Heidi Johansen-Berg,[1,2] Ned Jenkinson,[6] and Charlotte J. Stagg[1,2]

[1]Wellcome Centre for Integrative Neuroimaging, Functional MRI of the Brain, Nuffield Department of Clinical Neurosciences, University of Oxford, Oxford OX3 9DU UK, [2]Oxford Centre for Human Brain Activity, Wellcome Centre for Integrative Neuroimaging, Department of Psychiatry, University of Oxford, Oxford OX3 7JX, UK, [3]Medical Research Council Brain Network Dynamics Unit, Nuffield Department of Clinical Neurosciences, University of Oxford, Oxford OX1 3TH UK, [4]Department of Psychiatry, University of Oxford, Oxford OX3 7JX UK, [5]School of Health Sciences, Purdue University, Purdue, Indiana 47907, and [6]School of Sport, Exercise and Rehabilitation Sciences, University of Birmingham, Birmingham B15 2TT UK

Motor adaptation is crucial for performing accurate movements in a changing environment and relies on the cerebellum. Although cerebellar involvement has been well characterized, the neurochemical changes in the cerebellum underpinning human motor adaptation remain unknown. We used a novel magnetic resonance spectroscopic imaging (MRSI) technique to measure changes in the inhibitory neurotransmitter GABA in the human cerebellum during visuomotor adaptation. Participants (n = 17, six female) used their right hand to adapt to a rotated cursor in the scanner, compared with a control task requiring no adaptation. We spatially resolved adaptation-driven GABA changes at the cerebellar nuclei and cerebellar cortex in the left and the right cerebellar hemisphere independently and found that simple right-hand movements increase GABA in the right cerebellar nuclei and decreases GABA in the left. When isolating adaptation-driven GABA changes, we found that GABA in the left cerebellar nuclei and the right cerebellar nuclei diverged, although GABA change from baseline at the right cerebellar nuclei was not different from zero at the group level. Early adaptation-driven GABA fluctuations in the right cerebellar nuclei correlated with adaptation performance. Participants showing greater GABA decrease adapted better, suggesting early GABA change is behaviorally relevant. Early GABA change also correlated with functional connectivity change in a cerebellar network. Participants showing greater decreases in GABA showed greater strength increases in cerebellar network connectivity. Results were specific to GABA, to adaptation, and to the cerebellar network. This study provides first evidence for plastic changes in cerebellar neurochemistry during motor adaptation. Characterizing these naturally occurring neurochemical changes may provide a basis for developing therapeutic interventions to facilitate human motor adaptation.

Key words: **cerebellum; functional connectivity; GABA; neuroimaging; spectroscopy; visuomotor adaptation**

Received Jan. 10, 2022; revised June 9, 2022; accepted June 16, 2022.

Author contributions: C.N., N.J., H.J-B., and C.J.S. designed research; C.N., L.M., J.C., and C.J.S. performed research; W.T.C. and U.E. contributed unpublished reagents/analytic tools; C.N. and L.M. analyzed data; C.N. and C.J.S. wrote the paper.

This work was supported by the National Institute for Health Research (NIHR) Oxford Biomedical Research Center and the NIHR Oxford Health Biomedical Research Center. C.J.S. was supported by a Sir Henry Dale Fellowship, funded by the Wellcome Trust and Royal Society Grant 102584/Z/13/Z, and H.J-B. was supported by Wellcome Principal Research Fellowship 110027/Z/15/Z. The Wellcome Center for Integrative Neuroimaging is supported by core funding from the Wellcome Trust (Grant 203139/Z/16/Z).

The authors declare no competing financial interests.

Correspondence should be addressed to Caroline Nettekoven at cr.nettekoven@gmail.com.

https://doi.org/10.1523/JNEUROSCI.0096-22.2022

Significance Statement

Despite motor adaptation being fundamental to maintaining accurate movements, its neurochemical basis remains poorly understood, perhaps because measuring neurochemicals in the human cerebellum is technically challenging. Using a novel magnetic resonance spectroscopic imaging method, this study provides evidence for GABA changes in the left compared with the right cerebellar nuclei driven by both simple movement and motor adaptation. Although right cerebellar GABA changes were not significantly different from zero at the group level, the adaptation-driven GABA fluctuations in the right cerebellar nuclei correlated with adaptation performance and with functional connectivity change in a cerebellar network. These results show the first evidence for plastic changes in cerebellar neurochemistry during a cerebellar learning task. This provides the basis for developing therapeutic interventions that facilitate these naturally occurring changes to amplify cerebellar-dependent learning.

Introduction

As we move through the world, we are constantly confronted with changes in our bodies and our environment. Muscle properties change because of fatigue, exercise, or development, and the objects we interact with vary in weight, size, or how well we can manipulate them. Adapting our motor commands to these variations is thus crucial to interacting with our environment.

The cerebellum plays a key role in motor adaptation. Patient studies and brain stimulation suggest that an intact cerebellum function is a prerequisite for adaptation (Martin et al., 1996; Diedrichsen et al., 2005; Tseng et al., 2007; Jenkinson and Miall, 2010; Taylor et al., 2010), with more severe cerebellar impairment resulting in worse adaptation (Tseng et al., 2007). Healthy participants show increased cerebellar activity early in adaptation (Ichise et al., 2000; Seidler et al., 2006) and in response to sensory prediction errors (Schlerf et al., 2012), as well as adaptation-related changes in cerebellar activity in visuomotor learning paradigms (Miall and Jenkinson, 2005; Graydon et al., 2005). Although these studies provide a compelling argument for cerebellar involvement in adaptation, the physiological changes in the cerebellum during adaptation are not yet fully understood.

Adaptation may lead to decreases in the major inhibitory neurotransmitter GABA, which is found throughout the cerebellum and plays an important role in cerebellar plasticity (Ito, 2009). In the cerebellar cortex, GABA has been implicated in plasticity at parallel fiber synapses (Orts-Del'Immagine and Pugh, 2018) as well as Purkinje cell synapses (He et al., 2015). GABAergic Purkinje cells, the sole output neurons of the cerebellar cortex, exert a constant inhibitory tone on the deep cerebellar nuclei via frequent simple spike firing. Strong climbing fiber input causes Purkinje cells to fire complex spikes, resulting in a pause in simple spike firing, hence releasing the deep cerebellar nuclei from inhibition (Thach, 1967). In nonhuman primates, Purkinje cells increased complex spike firing, and therefore decreased inhibition, after introduction of a perturbation, which returned to baseline as the monkeys learned to adapt their movements, and errors decreased (Gilbert and Thach, 1977). However, despite the importance of GABA in motor adaptation, cerebellar GABA changes during human motor adaptation have not yet been investigated, likely because of the technical challenges presented by cerebellar MR in dealing with the low signal-to-noise ratio (SNR) in the cerebellum, which is located deep in the cranium and close to brainstem structures that move during the cardiac cycle (Diedrichsen et al., 2010; Brooks et al., 2013).

In this within-subject, crossover study, we used a novel magnetic resonance spectroscopic imaging (MRSI) approach to quantify GABA in the human cerebellum while participants performed a visuomotor adaptation task with their right hand, compared with a nonrotated control using the same hand. We were able to spatially resolve adaptation-driven GABA changes at the cerebellar nuclei and in the cerebellar cortex in the left and the right cerebellar hemispheres independently. We hypothesized that adaptation would lead to a decrease in GABA in the right deep cerebellar nuclei, as the uncrossed pathways at the level of the cerebellum results in mainly ipsilateral hand representations (Buckner et al., 2011; Mottolese et al., 2013; Diedrichsen and Zotow, 2015). We hypothesized that the degree of GABA decrease would be correlated with adaptation on a subject-by-subject basis so that greater GABA decreases related to greater adaptation. Finally, as previous studies have shown an increase in intrinsic functional connectivity in the cerebellum after adaptation (Albert et al., 2009; Nettekoven et al., 2020), and functional connectivity has been shown to correlate with GABA in a major network node (Stagg, 2014; Bachtiar et al., 2015), we hypothesized that GABA decrease would correlate with increased cerebellar functional connectivity.

Materials and Methods

Participants. Seventeen healthy right-handed participants (six female, 18–34 years, mean age 23 years) participated in this within-subject, crossover study. Each participant attended two sessions on two separate days during which they performed a visuomotor task with either an adaptation component (rotation condition) or no adaptation component (control condition) during MRI. The order of the sessions was counterbalanced across the group. Participants had no history of neurologic or psychiatric conditions and were not taking any psychoactive medications. All participants gave their written informed consent to participate, in line with central university research ethics committee approval (University of Oxford, R59564/RE002).

Experimental protocol. The experimental protocol for each session is shown in Figure 1*A*. Participants performed a visuomotor task using a hand-held joystick (custom-built fMRI joystick, 60 Hz sampling rate, Nata Technologies; Fig. 1*C*, left) to control a cursor on a screen, which either involved an adaptation component (rotation condition) or no adaptation component (control condition). Participants were instructed to make ballistic movements to shoot with their cursor through one of eight targets (Fig. 1*C*, middle).

The target appeared at one of eight locations radially aligned around the starting position of the cursor and separated by 45°. Trials were grouped into epochs, with one epoch containing eight consecutive trials and all blocks containing five epochs (total, $5 \times 8 = 40$ trials; one block equates to one gray shaded region in Fig. 1*B*). The sequence of target presentation was fixed across participants to ensure equal task difficulty across participants. Participants had to perform the movement within a time window of 750 ms, after which the target disappeared, to ensure short, ballistic movements, minimizing online corrections. No end point feedback was provided.

At the beginning of each session, participants performed a familiarization block outside the scanner, which consisted of 40 trials with no

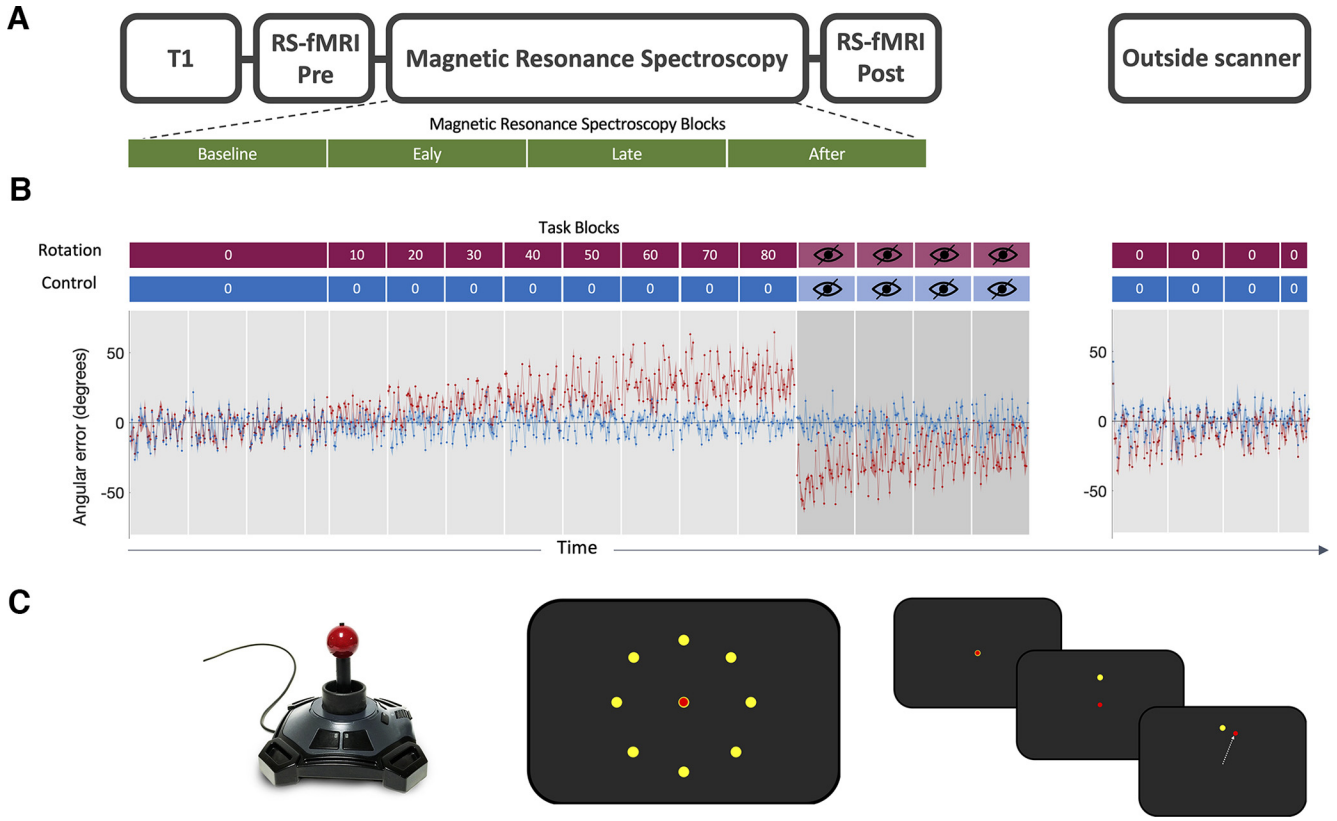

Figure 1. Experiment. ***A***, Scanning protocol. T1-weighted structural image was acquired at the beginning of the MRI scan. Resting-state fMRI data were acquired before and after the task. MRSI data were acquired during the task. Four MRSI scans were acquired during performance of the visuomotor task with each MRSI scan lasting 9 min, total acquisition time 36 min. ***B***, Behavioral data. Participants used a joystick to shoot targets on a screen. Participants began by performing 136 trials with no rotation imposed serving as the baseline in both conditions. In the rotation condition (red blocks), stepwise increase in rotated visual feedback required participants to adapt movements to reduce errors. One block at each angle and each block consisted of 40 trials of 4 s duration each. The numbers in the red and blue boxes indicate the degree to which the visual feedback was rotated, with 0° indicating no rotation. The imposed rotation reached a maximum of 80°, after which visual feedback was removed for four blocks of 40 trials each (blocks with crossed-out eye). In the control session (blue blocks), participants performed the task without any rotation imposed but for the same length (480 trials in total for the main task). The rotation was washed out after task (144 trials, no rotation). The task was practiced before the main task outside of the scanner (32 trials, no rotation; data not shown). Behavioral data are shown as angular error at each trial averaged across participants. Shaded area represents SEM. Rotation condition error is shown in red. Control condition error is shown in blue. Target sequence was fixed across participants and across sessions. ***C***, Task schematic. Left, MR-compatible joystick used to record participant responses. Middle, Eight possible target locations (yellow) centered radially around the cursor (red) at its starting position. Right, Schematic of a rotation trial. Cursor (red) is first presented at the center starting position. Target (yellow) appears at one of the eight possible target locations. Participant makes a center-out movement toward the target but sees clockwise-rotated visual feedback.

rotation imposed. They then performed 136 trials of no rotation in the scanner, serving as the baseline. Then, in the rotation condition, participants were required to adapt their centrifugal shooting movements to a rotation of the visual feedback, which increased stepwise by 10° after every block of 40 trials to maximally drive adaptation throughout the duration of the scanning session (Fig. 1*B*, red blocks). The imposed rotation reached a maximum of 80°, after which visual feedback was removed for four blocks of 40 trials each (blocks with crossed-out eye in Fig. 1*B*) to assess aftereffect. In the control condition, participants performed the task without any rotation imposed for the full duration of the task (Fig. 1*B*, blue blocks). After the scan, participants performed 144 trials (i.e., 3.6 blocks) with no rotation imposed to probe retention of the previously learned compensatory movement.

Behavioral analysis . Cursor movements were analyzed on a trial-by-trial basis using in-house software written in MATLAB (MathWorks). The joystick position data (X and Y) was collected at a sample rate of 60 Hz. The kinematic data were filtered with a zero-phase filter with a 25 Hz cutoff and numerically differentiated to determine velocity. Trials that showed premeditated or incomplete movements were excluded from further analysis (mean number of rejected trials, 30 ± 29).

For each trial, the angular error (measured in degrees) was calculated as the angle between a line connecting the starting position with the position of peak velocity of the cursor and the line connecting the starting position with the target. Positive values indicate a clockwise error (overshooting), and negative values indicate a counterclockwise error (undershooting).

We quantified adaptation in the rotation condition by calculating the mean error across all rotation blocks, excluding the first epoch of each block (Galea et al., 2011). We normalized the mean error in the rotation condition to the mean error in the control condition to ensure that differences in the adaptation measure were specific to better adaptation to the imposed rotation. To do this, we calculated error change in the rotation condition by dividing the angular error in rotation blocks by angular error at baseline. We then calculated the difference between error change in the rotation condition and error change in the control condition by subtracting control from rotation error change. Positive change values therefore reflect a greater increase in error in the rotation condition than in the control condition. The normalization formula applied to the rotation condition error was the same as the GABA normalization, which is described in a later section. We refer to this normalized rotation error as adaptation error in the following:

$$AdaptionError(timepoint) = \frac{error_{rotation}(timepoint)}{error_{rotationbaseline}} - \frac{error_{control}(timepoint)}{error_{controlbaseline}}$$

To quantify aftereffect, the mean error during all open loop trials of the rotation condition was normalized to the mean error during the control condition open loop trials. We refer to this normalized open loop measure as aftereffect. To quantify retention, the mean error in the first washout block of the rotation condition was normalized to the mean error in the first washout block after the control condition. We refer to this normalized washout error as retention error.

To determine whether participants adapted in the rotation condition, we used the lme4 package in R software (Bates et al., 2015) to construct a linear mixed-effects model (LME) of error with epoch and target as fixed effects. To directly compare error reduction from the beginning of each block to the end of each block in the rotation condition and in the control condition, we constructed an LME model of the first and last epoch error in both conditions and tested for a significant condition times epoch interaction. In this LME model, we also entered target as a fixed effect to account for target-specific movement biases. For all LME models we allowed intercepts for different subjects to vary, to account for covarying residuals within subjects.

Neuroimaging acquisition. All magnetic resonance data were acquired on a 3T Siemens scanner (Prisma) with a 32-channel head coil. Structural MRI data were acquired using a magnetization-prepared rapid acquisition gradient echo (MPRAGE) sequence (TR = 1900 ms, TE = 3.96 ms, slice thickness 1.0 mm, in-plane resolution 1.0 × 1.0 mm^2, flip angle = 8, FOV = 256 × 232 mm^2). The resting-state fMRI acquisition was matched to the UK Biobank resting-state fMRI parameters described in Alfaro-Almagro et al. (2018). A multiband isotropic EPI acquisition (TR/TE = 735/39 ms, FOV = 210 × 210 mm^2, bandwidth = 2030 Hz/pixel, multiband acceleration factor 8, voxel dimension = 2.4 × 2.4 × 2.4 mm^3; whole brain, acquisition time = 6:10 min for a total of 490 volumes) was performed before and immediately after the task. A separate single-band reference scan (SBRef) was acquired before the multiband acquisition (Moeller et al., 2010). This serves as the reference scan during preprocessing (e.g., during motion correction and registration steps) as it suffers from the same distortions as the multiband data but has higher contrast (Alfaro-Almagro et al., 2018). Subjects fixated on a cross-hair image presented centrally on the screen during resting-state fMRI acquisition.

fMRI analysis. All MRI data processing was conducted using Functional MRI of the Brain (FMRIB) Software Library, (version 6.00; Jenkinson et al., 2012). For resting-state functional data, preprocessing steps were largely matched to the UK Biobank processing pipeline (Alfaro-Almagro et al., 2018). The data were motion corrected using MCFLIRT (the FMRIB Linear Registration Tool; Jenkinson et al., 2012), slice-timing corrected using Fourier-space time series phase-shifting, distortion-corrected using fieldmaps (B0 unwarping), stripped of nonbrain voxels using BET (Brain Extraction Tool; Smith, 2002), grand-mean intensity normalized and high-pass temporally filtered (Gaussian-weighted least-squares straight line fitting, with σ = 50.0 s).

To remove structured noise, functional data were cleaned using a single-subject independent components analysis (ICA), implemented in MELODIC (Multivariate Exploratory Linear Optimized Decomposition into Independent Components) and the automated classifier FIX, which was trained on 40 hand-labeled Biobank datasets to identify noise ICA components (Beckmann and Smith, 2004; Griffanti et al., 2014; Salimi-Khorshidi et al., 2014). Although these training datasets were matched in acquisition sequence and experimental parameters to the datasets acquired in our experiment, we checked their classification accuracy to ensure the suitability of the Biobank-trained FIX algorithm for our data by manually classifying four datasets and comparing our labels to the FIX classification. The FIX-classified labels matched our hand classification at 99.8%, which is within the expected range of classification accuracy (Alfaro-Almagro et al., 2018).

Functional data were registered to the MNI-152 template, using the SBref image as an intermediate step. Functional data were first linearly registered to the SBref image using six degrees of freedom (FLIRT; Jenkinson and Smith, 2001; Jenkinson et al., 2002), then to the structural image using boundary-based registration (implemented in FLIRT), and finally to the MNI-152 template using nonlinear registration (FNIRT; Andersson et al., 2007, 2019). Finally, spatial smoothing was applied with a 5 mm FWHM Gaussian kernel.

Group networks. To derive group networks, we applied a group ICA. For this, we concatenated the preprocessed functional data temporally across sessions and across subjects to create a single dataset. We then used the group ICA to obtain 50 components. Visual inspection of the group-level components revealed that at a dimensionality of 50 the cerebellar network of interest included only cerebellar regions, whereas at a lower dimensionality, this network included regions of the visual cortex. We confirmed the cerebellar network (see Fig. 5*A*) as the network with the greatest spatial correlation with cerebellar regions active during performance of sensorimotor tasks (Hardwick et al., 2013). To determine the anatomic specificity of any effects, we identified the default mode network (DMN; see Fig. 5*B*) as a control network, which we expected to be unaffected by task condition and does not spatially overlap with the task activation mask.

Dual regression. Subject-and-scan-specific networks were obtained via a dual regression approach (Nickerson et al., 2017), masked by the group mean network.

Connectivity change. We tested whether change in network strength correlated with change in GABA. We obtained the network strength measure from the subject-and-scan-specific networks, which were derived through dual regression. Those networks were then masked by the group mean network and the within-mask z values were extracted and averaged. This resulted in one value, which reflects the network strength for each subject and for each fMRI time point (pre and post), from which we then calculated strength change. To do this, we used the same normalization procedure as the one used for behavioral data, namely dividing the strength value of the network of the subject after task performance (Fig. 1*A*, post) by network strength at baseline (Fig. 1*A*, pre) and calculating the difference between rotation strength change and control strength. Positive change values therefore reflect a greater increase in network strength in the rotation condition than in the control condition. We refer to this measure as connectivity change.

Spectroscopic imaging acquisition. Structural images were used to manually place a 65 × 25 × 15 mm^3 MRSI slab in the cerebellum. The slab was positioned to cover anterior and superior areas of the right cerebellum that contain the hand motor representation (Buckner et al., 2011; Mottolese et al., 2013; Diedrichsen and Zotow, 2015) while avoiding contact with either the dura, to minimize significant macromolecule contamination, or with brainstem, to avoid excess physiological noise (Brooks et al., 2013).

Four MRSI scans were acquired during performance of the visuomotor task (time per scan, 9 min; total acquisition, 36 min; TE = 32 ms; Fig. 1*A*). MRSI data were acquired using a nonwater suppressed semi-LASER DW-CRT (density weighted concentric ring trajectory) sequence with metabolite cycling (Steel et al., 2018) at 5 × 5 × 15 mm^3 resolution.

Spectroscopy analysis. MRSI data were reconstructed and preprocessed according to Steel et al. (2018) using in-house scripts. Briefly, preprocessing included the following: metabolite cycling reconstruction (Emir et al., 2017), coil-combination (Walsh et al., 2000), correction for frequency and phase shifts, residual water removal using Hankel-Lanczos singular value decomposition (Cabanes et al., 2001), and eddy currents correction using the unsuppressed water signal (Klose, 1990). Concentration of neurochemicals was quantified as in Steel et al. (2018), using LCModel software (Provencher, 2001). Specifically, we used a chemical shift of 0.5–4.2 ppm, a basis set containing 30 metabolites, default LCModel macromolecules, soft constraints on metabolites that were disabled, and a baseline stiffness setting (DKMTM) of 0.25 (raw spectrum, spectral fit, and scaled basis spectra in Fig. 2*C*). Voxels in the metabolite maps were excluded if the Cramer-Rao lower bounds of the respective metabolite > 60%, LCModel defined line widths (FWHM) > 20 Hz, or SNR < 15 (Fig. 2*A*, thresholded GABA shown in maps). MRSI data analysis therefore yielded independent quantification of neurochemical concentrations at four time points. All neurochemical concentrations are expressed as a ratio to total Creatine (Cr + PCr, tCr).

Metabolite maps were registered to the MNI template by a linear registration to the structural scan (FLIRT; Jenkinson and Smith, 2001; Jenkinson et al., 2002) and then nonlinearly warp to the MNI template (FNIRT; Andersson et al., 2007, 2019). Overlap maps of the MRSI slab in MNI space for each condition are shown in Figure 2*B*. The MRSI slab was reproducibly placed between sessions (mean spatial correlation coefficient between each subject's pair of MRS voxels, r = 0.85 ± 0.06). The MRSI slab overlapped on average with 22% of participant's right cerebellar lobule VI (mean, 22 ± 6.29%) and with 20.6% of the right cerebellar lobule VI (mean, 20.6 ± 6.87%). There was no significant difference between left

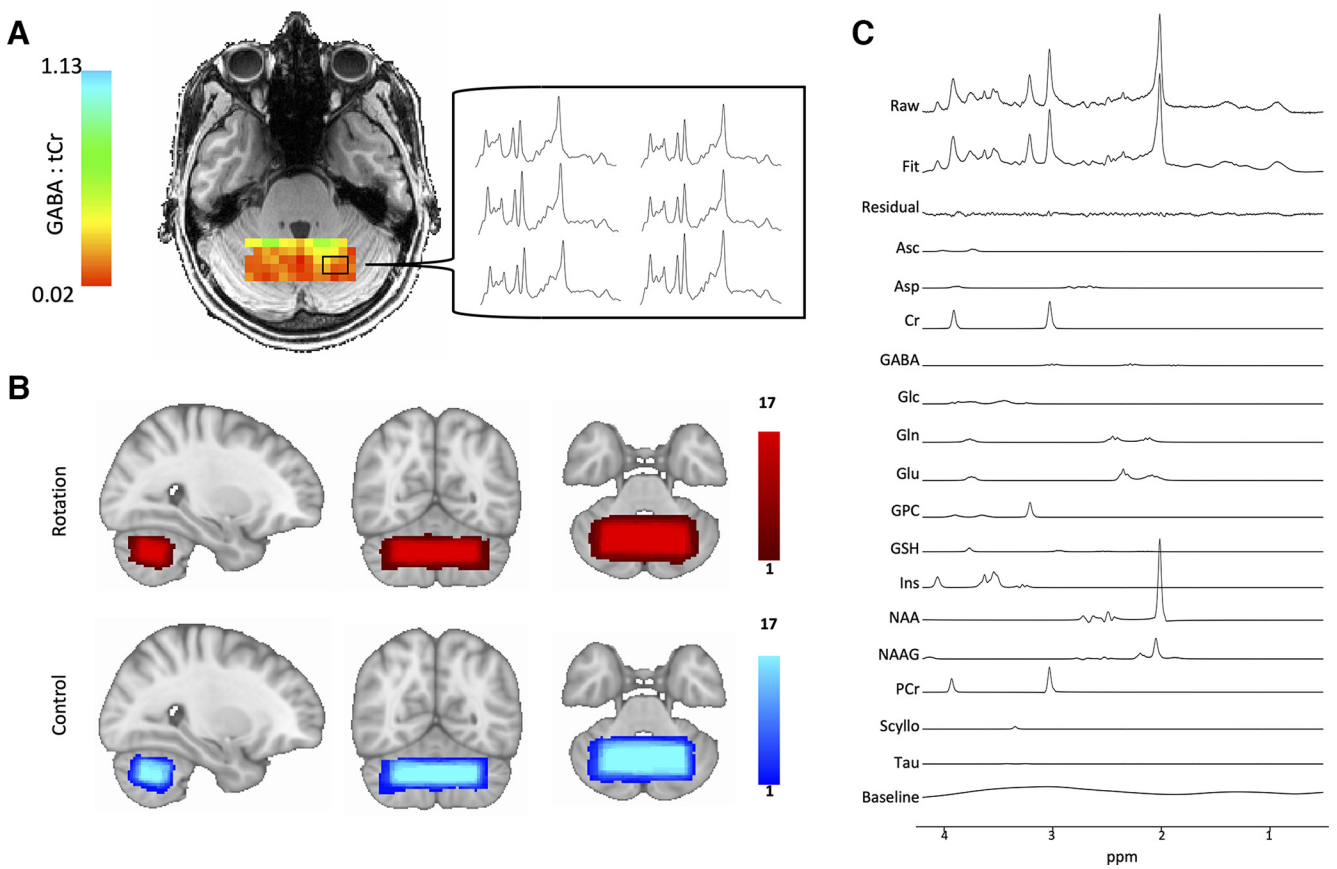

Figure 2. Cerebellar magnetic resonance spectroscopic imaging. ***A***, Representative GABA map. Image shows representative GABA map for one subject after quality control thresholding including the individual MRSI spectra from six voxels that allow quantification of GABA concentration in each voxel. Left, Color bars show GABA:tCr concentration in each voxel. ***B***, Voxel placement. MRSI voxel overlap maps for the two conditions. A $65 \times 25 \times 15$ mm^3 MRSI slab placed over the anterior and superior areas of the cerebellum so that it optimally covers the right-hand motor representation. Right, Color bars indicate number of participants. ***C***, Spectral fit. Image shows representative spectra of one subject including LCModel fit. Metabolite basis spectra have been scaled using LCModel so that a linear combination of the basis spectra, the residual, and the baseline best fits the raw measured spectrum. Top, Measured raw spectrum. Bottom, LCModel fit. GABA metabolite peaks appear at 1.89, 2.29, and 3.01 ppm.

lobule VI coverage compared with right lobule VI coverage (paired *t* test of percentage values, $t_{(16)} = 0.68$, $p = 0.51$). Hence, coverage of the left and right cerebellar lobules was similar and did not systematically differ, ensuring that the measurements were not biased to either hemisphere.

To address our hypotheses, we conducted a region-of-interest (ROI)-based analysis using the SUIT toolbox (Diedrichsen, 2006) for SPM12 (Statistical Parametric Mapping 12) software. We created SUIT-space ROIs for the left and right cerebellar nuclei and cortex separately (Fig. 3*C*, right, *I*, right). We then registered the SUIT-space ROI masks to each subject's structural scan (Emir et al., 2021). The nuclei masks consisted of all deep cerebellar nuclei of the respective hemisphere. Because resolving GABA changes at the level of individual nuclei is not currently feasible, we did not perform the analysis at the level of individual nuclei but rather quantified GABA from masks that include all deep cerebellar nuclei in the right and the left hemisphere; that is, for the right hemisphere the mask included the right dentate, the interposed and fastigial nuclei. The fastigial nucleus was included because animal studies have suggested that the output of the fastigial nucleus is relevant for upper limb movement (Bava et al., 1983; Licata et al., 1985).

Normalization. To control for movement effects, we normalized GABA in the rotation condition to GABA in the control condition using the same normalization procedure as was applied to the behavioral data:

$$GABA_{Normalised}(timepoint) = \frac{GABA_{rotation}(timepoint)}{GABA_{rotationbaseline}} - \frac{GABA_{control}(timepoint)}{GABA_{controlbaseline}}$$

The normalized GABA value at each time point is therefore equivalent to taking the difference between the percentage change in rotation GABA and the percentage change in control GABA. The GABA data were normalized for each hemisphere separately, resulting in normalized values for left and right cerebellar hemispheres ($GABA_{Left}$ and $GABA_{Right}$, respectively).

Statistical analysis. Mean ± SD is presented throughout. Statistical analyses of the data were conducted using R software (http://www.r-project.org) and Statistics Package for the Social Sciences (SPSS, version 25, IBM). Repeated measures ANOVAs were used to test for neurochemical changes in the cerebellum during the different experimental conditions in the left compared with the right cerebellum. Maunchly's test of sphericity was used to test the homogeneity of variance. Where Mauchly's test of sphericity was significant ($p < 0.05$) in repeated measures ANOVAs, Greenhouse–Geisser corrections were applied. *Post hoc* tests were calculated using Bonferroni-adjusted paired samples *t* tests.

To test relationships between neurochemical changes and behavior, Pearson's correlation coefficients (two tailed) were calculated. Partial correlations were used to control for a behavioral index of no interest (two tailed, unless otherwise specified). To determine whether two correlation coefficients were significantly different, Pearson's correlation coefficients were converted into *z* scores using Fisher's *Z*-transformation. One-tailed z tests were then performed on the *z* scores, given the standard error of each *z* score (Myers and Sirois, 2006).

Data availability. MRI data, MRSI data and behavioural will be shared on the data sharing platform of the Wellcome Centre for Integrative Neuroimaging which is currently under development. In the interim, data is available upon request.

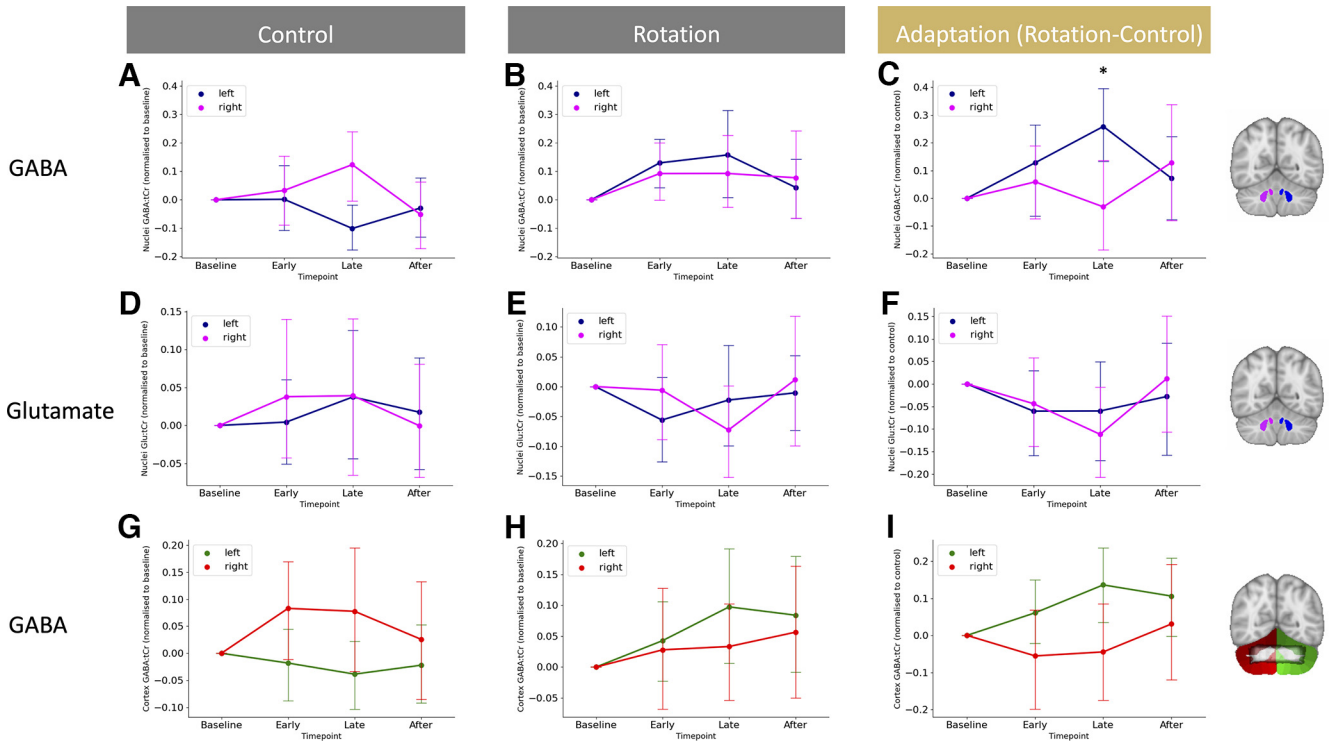

Figure 3. Isolating adaptation reveals GABA diverges in the left and right cerebellar nuclei. ***A***, GABA changes in the cerebellar nuclei during movement execution. Shown are GABA values normalized to baseline in the control condition. ***B***, No GABA changes in in the left and right cerebellar nuclei while participants are in the rotation condition. Shown are GABA values normalized to baseline in the rotation condition. ***C***, Adaptation-driven GABA changes in the left and right cerebellar nuclei. Against a backdrop of GABA changes related to simple movement execution, GABA diverges in the left and right cerebellar nuclei driven by adaptation. ***D–F***, Glutamate does not change in the left and right cerebellar nuclei during the control condition (***D***), rotation condition (***E***), or when isolating adaptation (***F***). ***G–I***, GABA does not change in the left and right cerebellar cortex during the control condition (***G***), rotation condition (***H***), or when isolating adaptation (***I***). For visualization purposes, data in left and middle columns are shown normalized to baseline. Statistics for control and rotation data were conducted on raw, non-normalized data. Statistics testing for adaptation-driven changes were calculated on rotation data normalized to control data. The inset in ***I*** shows the overlap between cerebellar cortex ROI for the left (green) and the right (red) with an overlay mask of the MRSI slab from all sessions (shown in black at 50% opacity). The MRSI slab overlaps with the hand representation in lobule VI bilaterally and in the right lobule V. Error bars show ± standard error. Asterisk (*) indicates significant point times hemisphere interaction in isolated adaptation.

Results

Participants adapted in the rotation condition and retained the aftereffect

We first tested whether participants adapted by reducing their error to the applied visuomotor perturbation in the rotation condition. As expected, we found that participants adapted within rotation blocks, indicated by a significant effect of epoch on error [LME of error in rotation blocks, $\chi 2(1) = 5.78$, $p = 0.02$; Fig. 1*B*]. To test whether this error reduction was specific to the rotation condition, we then compared error reduction in the rotation condition and error reduction in the control condition directly. In line with error reduction taking place exclusively in the rotation blocks of the rotation condition, we observed a significant interaction of epoch and condition in an LME [$\chi 2(1) = 12.697$, $p < 0.001$].

We next tested whether participants retained the adapted state. We observed an aftereffect in each of the four open loop blocks of the rotation condition, indicated by a significant negative error (Bonferroni-corrected one-sample t test of mean error for each open loop block, all p values < 0.001). In contrast, no aftereffect was observed in any of the open loop blocks of the control condition (Bonferroni-corrected one-sample t test of mean error for each block, all p values > 0.99). Directly comparing the open loop blocks of the rotation condition and the control condition confirmed the presence of an aftereffect throughout the open loop blocks (Bonferroni-corrected paired t test of mean error for each open loop block, all p values < 0.001; Fig. 1*B*).

We found that participants retained the compensatory movement in the washout phase of the rotation condition (Bonferroni-corrected one-sample t test of mean error for each block, all p values < 0.01), but there was no error during the washout phase of the control condition (Bonferroni-corrected one-sample t test of mean error for each block, all p values > 0.28).

Because the rotation task imposed an adapted state that persisted throughout the washout phase, we tested for potential carryover effects from the rotation session to the next session in this counterbalanced study. We found no evidence for carryover effects in the second session as there was no difference in baseline error of the second session between participants who had performed the rotation condition in the first session and participants who had performed the control condition in the first session (paired t test of baseline error, -4.090 ± 0.536, $t_{(15)} = -1.760$, $p = 0.099$).

GABA is stable across sessions

Because the MRSI approach used in this study has not been used before in the cerebellum, we first quantified the reliability of our GABA measurements at baseline across sessions. The intraclass-correlation coefficient of the baseline GABA measurements was 0.45 ($F_{(16,16.5)} = 2.63$, $p = 0.03$), indicating a fair reliability between sessions. To check whether GABA quantification was affected by the number of MRSI voxels included in an ROI, we looked for a relationship between GABA:tCr and number of voxels in our ROIs and found no relationship in either the deep cerebellar nuclei

masks ($r = -0.13$, $p = 0.29$) or the cerebellar cortex masks ($r = -0.1$, $p = 0.42$). Further, there was no difference in the number of voxels surviving quality assessment across the slab between the two conditions ($t_{(16)} = 1.140$, $p = 0.27$).

GABA changes in the cerebellar nuclei during movement execution

We first investigated GABA changes over time between conditions, regions, and hemispheres, via a four-way repeated-measures ANOVA with within-subject factors of condition (Rotation, Control), region (Nuclei, Cortex), hemisphere (Left, Right) and time point (Base, Early, Late, After). There was no main effect on GABA:tCr of condition ($F_{(1,16)} = 1.145$, $p = 0.300$, partial $\eta 2 = 0.067$) or time point ($F_{(3,48)} = 1.391$, $p = 0.257$, partial $\eta 2 = 0.08$). However, GABA:tCr differed between regions ($F_{(1,16)} = 463.532$, $p < 0.0001$, partial $\eta 2 = 0.967$) and between hemispheres ($F_{(1,16)} = 71.816$, $p < 0.0001$, partial $\eta 2 = 0.818$), with higher GABA:tCr in the cerebellar nuclei (0.554 ± 0.014) than in the cerebellar cortex (0.348 ± 0.012) and higher GABA:tCr in left (0.478 ± 0.013) compared with the right cerebellar hemisphere (0.424 ± 0.012). There was a significant interaction between region and hemisphere ($F_{(1,16)} = 21.403$, $p < 0.001$, partial $\eta 2 = 0.572$), driven by a greater difference in GABA:tCr between the hemispheres in the nuclei than in the cortex. Finally, we observed a significant three-way interaction among condition, hemisphere, and time point ($F_{(3,48)} = 4.544$, $p = 0.007$, partial $\eta 2 = 0.221$). All other interactions were nonsignificant (all p values > 0.1).

To understand this three-way interaction, we performed repeated-measures ANOVAs on GABA:tCr from the two conditions and the two regions separately, with within-subject factors of hemisphere (Left, Right) and time point (Base, Early, Late, After; Fig. 3).

In the control condition, there were no bilateral task-related changes in GABA:tCr in the cerebellar nuclei (main effect of time point, $F_{(3,48)} = 0.793$, $p = 0.504$, partial $\eta 2 = 0.047$), but there was a significant main effect of hemisphere ($F_{(1,16)} = 9.551$, $p = 0.007$, partial $\eta 2 = 0.374$) and a significant hemisphere times time interaction ($F_{(3,48)} = 3.943$, $p = 0.014$, partial $\eta 2 = 0.198$; Fig. 3*A*). *Post hoc t* tests demonstrated that GABA:tCr was higher in the left than right nuclei at baseline ($t_{(16.000)} = 3.552$, $p = 0.011$, 0.829 ± 0.963). However, during control task performance, GABA decreased in the left nuclei and increased in the right nuclei, so there was no significant difference between the hemispheres during task performance (Early, $t_{(16.000)} = 2.204$, $p = 0.170$, 0.636 ± 1.190; Late, $t_{(16.000)} = -0.438$, $p = 1.000$, -0.125 ± 1.179; Fig. 3*A* shows GABA:tCr time course normalized to baseline). In the cerebellar cortex, performance of the control task had no significant effects on GABA:tCr (main effect of hemisphere, $F_{(1,16)} = 3.166$, $p = 0.094$, partial $\eta 2 = 0.165$; main effect of time point, $F_{(3,48)} = 0.793$, $p = 0.275$, partial $\eta 2 = 0.017$; hemisphere times time interaction, $F_{(3,48)} = 3.943$, $p = 0.277$, partial $\eta 2 = 0.074$; Fig. 3*G*).

In the rotation condition, there were no task-related changes in GABA:tCr in the cerebellar nuclei (main effect of time point, $F_{(3,48)} = 2.528$, $p = 0.068$, partial $\eta 2 = 0.136$; hemisphere times time interaction, $F_{(3,48)} = 0.539$, $p = 0.658$, partial $\eta 2 = 0.033$; Fig. 3*B*) or the cortex (main effect of time point, $F_{(3,48)} = 0.644$, $p = 0.591$, partial $\eta 2 = 0.039$; hemisphere times time interaction, $F_{(3,48)} = 0.539$, $p = 0.658$, partial $\eta 2 = 0.033$; Fig. 3*H*).

Isolating adaptation reveals GABA diverges in the left and right cerebellar nuclei

Given the significant effects of movement on GABA:tCr in the cerebellar nuclei, we wished to isolate any effects of adaptation over and above movement on inhibition. In particular, we wanted to account for any GABA fluctuations not driven by adaptation but by movement execution or other learning processes such as use-dependent learning. To do this we normalized GABA:tCr during the rotation condition to GABA:tCr during control by subtraction (Fig. 3*C*,*I*). To test the hypothesis that GABA would be differentially affected in the left and right nuclei during adaptation, we then performed a two-way repeated-measures ANOVA with within-subject factors of hemisphere (Left, Right) and time point (Early, Late, After). In line with our hypothesis, we observed significant GABA:tCr modulation in left compared with right nuclei (significant hemisphere times time interaction, $F_{(2,32)} = 4.490$, $p = 0.014$, partial $\eta 2 = 0.236$; main effect of time point, $F_{(2,32)} = 0.054$, $p = 0.948$, partial $\eta 2 = 0.003$; Fig. 3*C*).

Finally, to test the neurochemical specificity of the observed GABA:tCr changes in the cerebellar nuclei, we performed an equivalent repeated-measures ANOVA to investigate adaptation-related changes in Glutamate:tCr. There was no main effect of time point on Glutamate:tCr, and no hemisphere times time interaction (main effect of time point, $F_{(2,32)} = 0.054$, $p = 0.948$, partial $\eta 2 = 0.003$; $F_{(2,32)} = 4.490$, $p = 0.014$, partial $\eta 2 = 0.236$; Fig. 3*F*), suggesting that these findings were specific to GABA and not a reflection of more general processes.

Additionally, although not the main focus of the experiment, we tested for GABA changes for each hemisphere separately. For this, we used a one-sample *t* test of GABA change from baseline to time point Late separately for each condition and each hemisphere. In the control condition, there was a significant GABA change in the left cerebellar nuclei ($t_{(16)} = -2.46$, $p = 0.03$) and a nonsignficant GABA change in the right cerebellar nuclei ($t_{(16)} = 1.88$, $p = 0.08$). In the rotation condition, there was no significant GABA change in the right cerebellar nuclei ($t_{(16)} = 1.36$, $p = 0.19$) or in the left cerebellar nuclei ($t_{(16)} = 1.98$, $p = 0.07$). GABA change during isolated adaptation was significantly different from zero for the left cerebellar nuclei ($t_{(16)} = 3.75$, $p < 0.002$) but not for the right cerebellar nuclei ($t_{(16)} = -0.38$, $p = 0.14$).

Adaptation-driven early GABA change correlates with adaptation

Prior studies have shown that early change in motor cortical GABA during learning of a motor sequence correlates with subsequent learning-related changes in reaction times on the task (Kolasinski et al., 2019; Floyer-Lea et al., 2006). We therefore hypothesized that early change in the right cerebellar nuclei GABA:tCr would correlate with error during adaptation. We observed a significant correlation between change in GABA:tCr in the right nuclei and adaptation error (Fig. 4*B*; $r = 0.64$ $p = 0.006$), in that participants showing an early decrease in right nuclei GABA:tCr (time point, Early; Fig. 1*A*) adapted their right-hand movements better to the rotation. This relationship was specific both neurochemically (change in Glutamate:tCr and adaptation, $r = -0.10$, $p = 0.693$; zdiff = 2.27, $p = 0.011$; Fig. 4*C*) and anatomically (change in left nuclei GABA:tCr and adaptation, $r = -0.16$, 0.537; zdiff = 2.43, $p < 0.01$). To test whether our relationship between GABA:tCr and adaptation was specific to that behavior, we tested for a relationship between GABA:tCr change and retention error, which demonstrated a significant correlation ($r = -0.49$, $p = 0.0455$). However, as expected, our metrics of adaptation and retention are highly correlated ($R = -0.8185$, $p < 0.0001$). We therefore calculated partial correlations between early GABA:tCr change and the two behavioral metrics. GABA:tCr change and adaptation were still significantly correlated when controlling for retention (r

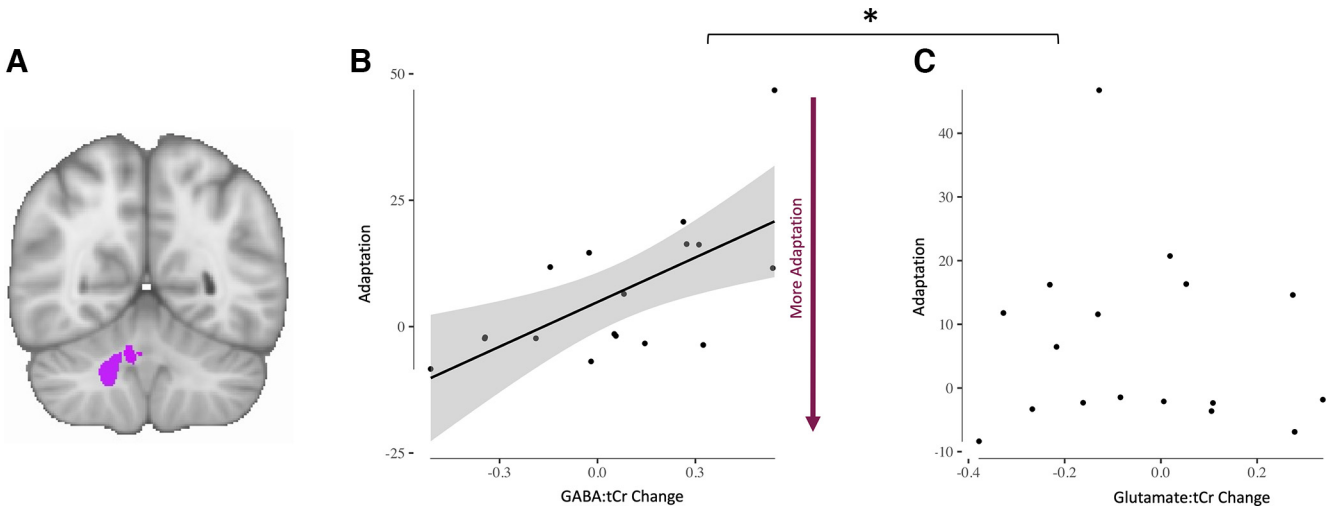

Figure 4. Adaptation-driven early GABA change correlates with adaptation. ***A***, Right cerebellar nuclei ROI. ***B***, GABA change in right cerebellar nuclei correlates with adaptation ($r = 0.64$, $p = 0.006$). Each dot represents one participant. Shading indicates 95% confidence bounds of the relationship. ***C***, Glutamate change in right cerebellar nuclei does not correlate with adaptation ($r = -0.10$, $p = 0.693$). Each dot represents one participant. Line of best fit is not plotted for this correlation because the correlation is not significant. The asterisk (*) Indicates that the relationships were significantly different (GABA change vs glutamate change relationship; zdiff = 2.27, $p = 0.011$).

= 0.47, $p = 0.03$, one tailed), but GABA:tCr change did not correlate with retention when controlling for adaptation ($R = 0.07$, $p = 0.39$). Additionally, we tested whether GABA change from baseline to time point Early was significantly different from zero. We found no significant difference ($t_{(16)} = 0.81$, $p = 0.43$).

Adaptation-driven GABA changes correlate with cerebellar connectivity change

Finally, we wanted to determine whether our behavior-related changes in GABA correlated with changes in cerebellar functional connectivity. We did not demonstrate a significant group mean change in cerebellar network strength after adaptation (all p values > 0.05). However, there was a significant correlation between early change in right nuclei GABA:tCr and the change in cerebellar functional connectivity ($r = -0.4939$, $p = 0.0439$; Fig. 5*D*). This relationship was both neurochemically (glutamate change and cerebellar connectivity change, $r = 0.09$, $p = 0.71$; zdiff = −1.69 $p = 0.0459$; Fig. 5*E*) and anatomically specific (GABA change and connectivity change in default mode network (DMN), $r = 0.2707$, $p = 0.29$; zdiff = −2.17, $p = 0.015$; Fig. 5*C*). There was no relationship between cerebellar connectivity change and adaptation error ($r = -0.11$, $p = 0.67$).

Discussion

In this study, we used a novel, spatially resolved MRSI technique to quantify cerebellar GABA to investigate neurochemical changes during visuomotor adaptation. We found that simple movement of the right hand leads to diverging GABA time courses in the right cerebellar nuclei compared with GABA in the left. When controlling for these movement-related GABA changes, in line with our hypotheses, we found GABA in the left cerebellar nuclei increased compared with GABA in the right cerebellar nuclei during adaptation. Although GABA change from baseline at the right cerebellar nuclei was not different from zero at the group level, early adaptation-driven fluctuations in right cerebellar nuclei GABA correlates with performance in the right-hand adaptation task. Participants who show a greater GABA decrease adapt better, suggesting this early GABA change is behaviorally relevant. Finally, although we did not demonstrate a group mean change in cerebellar connectivity, the adaptation-driven right cerebellar nuclei GABA decrease correlated with functional connectivity changes in a network that has previously been shown to increase in strength in response to adaptation (Albert et al., 2009; Nettekoven et al., 2020). Participants who show a greater early decrease in GABA in the right cerebellar nuclei also show a greater increase in cerebellar network connectivity. These findings are anatomically specific and neurochemically specific; control analyses show no adaptation-related changes in the cerebellar cortex and no concentration changes in glutamate. Our results are also behaviorally specific and network specific. The relationship between adaptation and right nuclear GABA change holds when controlling for retention, but there is no correlation between retention and right nuclear GABA change controlling for adaptation, suggesting this relationship is specific to adaptation. Further, right nuclear GABA change correlates with strength change in a cerebellar network but not with strength change in the default mode network, confirming the specificity of our results for functional connectivity of the cerebellum.

Movement-related increase in GABA in ipsilateral nuclei

When groups of parallel fibers activate and cause high enough input to Purkinje cells so that Purkinje cells fire simple spikes, this results in GABA release at the cerebellar nuclei. Simple spike responses can occur in response to a large variety of vestibular and motor signals *in vivo* (Dean et al., 2010; Barmack and Yakhnitsa, 2013). For example, increases in simple spike firing have been shown during eye movements in the direction of their preferred response (Medina and Lisberger, 2008; Yang and Lisberger, 2014). There may also be population coding of hand movements within the complex spike (CS) as has been described for eye movements (Thier et al., 2000; Popa et al., 2019).

Although the increase in GABA in the right compared with the left cerebellar nuclei observed in this study was unexpected, there are a number of plausible reasons for this GABA change during simple movement execution. Perhaps the most parsimonious explanation would be that GABA increase in the right nuclei could reflect increased simple spike firing of Purkinje cells,

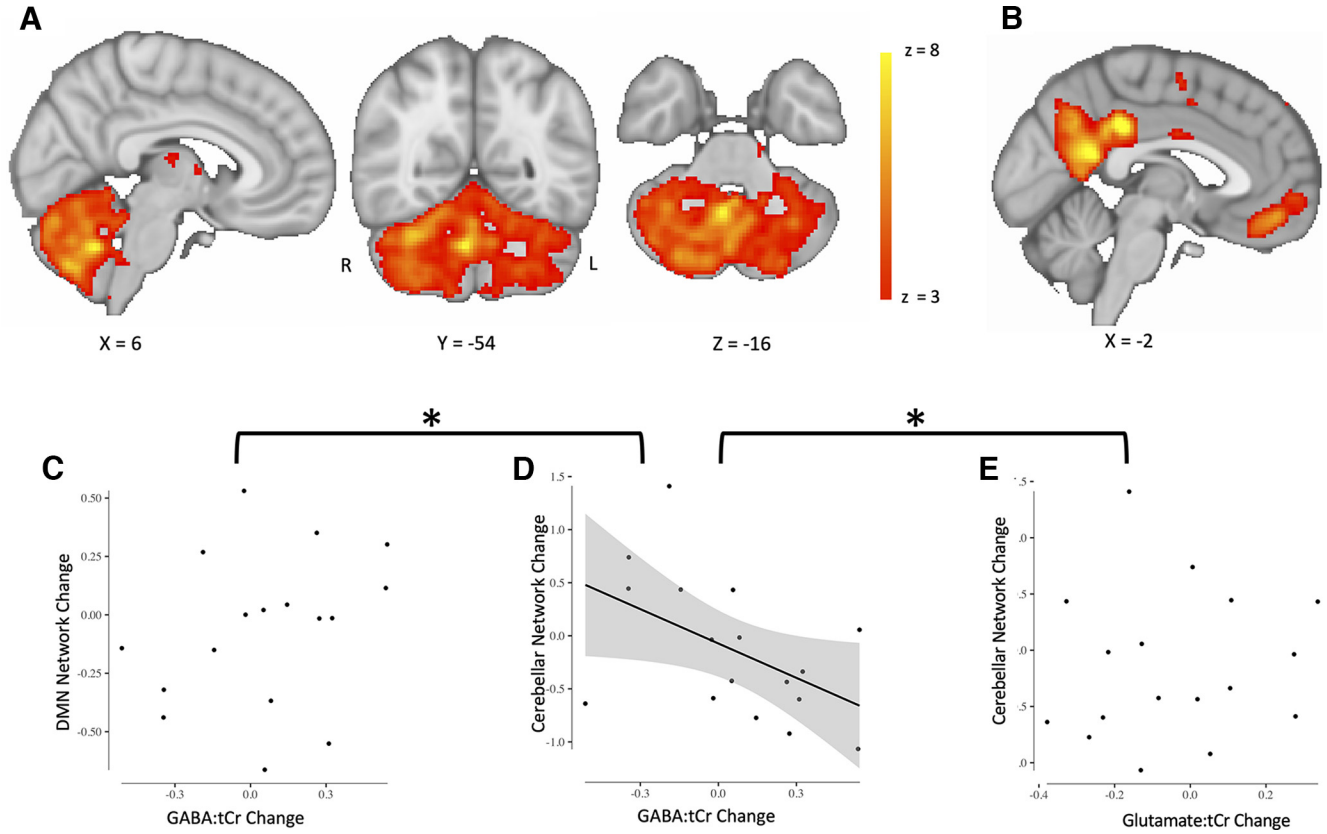

Figure 5. Adaptation-driven GABA changes correlate with cerebellar connectivity change. ***A***, Cerebellar network. Cerebellar network that has previously been found to increase in connectivity after adaptation is shown in red-yellow. Right, Color bar indicates range of *z* values in voxels. Brain slices are shown according to radiology convention; left hemisphere is shown on the right, indicated by R (right) and L (left) surrounding the coronal slice. ***B***, The DMN was chosen as a control network. ***C***, Change in default mode network strength does not correlate with GABA change in right cerebellar nuclei ($r = 0.2707$, $p = 0.29$). Data points represent individual participants. Line of best fit is not plotted for this correlation because the correlation is not significant. ***D***, Change in cerebellar network strength correlates with GABA change in right cerebellar nuclei. Participants who show a greater decrease in early GABA in the right cerebellar nuclei also show a larger increase in cerebellar network strength ($r = -0.4939$, $p = 0.0439$). Cerebellar network strength decreases in participants who show an increase in GABA in the right cerebellar nuclei. Data points represent individual participants. Plot shows line of best fit for correlation and 95% confidence interval. ***C–E***, Change in cerebellar network strength does not correlate with glutamate change in right cerebellar nuclei ($r = 0.09$, $p = 0.71$). Data points represent individual participants. Line of best fit is not plotted for this correlation because the correlation is not significant. The asterisk (*) indicates significant difference between correlations shown in ***C*** and in ***D*** as well as in ***D*** and ***E***. The correlation coefficient of cerebellar network change and GABA change was significantly different from the correlation coefficient of DMN change and GABA change (zdiff = −2.17, $p = 0.015$). The correlation coefficient of cerebellar network change and GABA change was also significantly different from the correlation coefficient of cerebellar network change and glutamate change (zdiff = −1.69, $p = 0.0459$).

leading to higher GABA concentration in the deep cerebellar nuclei. In the control condition, participants performed simple ballistic wrist movements with veridical visual feedback, and participants therefore made no systematic movement errors. In response to these simple movements, converging parallel fiber activity may have caused Purkinje cells in the right cerebellum to fire simple spikes, and because of the absence of movement errors in the control condition, a lack of complex spikes may have increased simple spike activity of the same Purkinje cells.

Adaptation-related change in GABA in ipsilateral nuclei

Unexpected target movements that result in a visual error have been shown to lead to complex spike firing on some trials (Medina and Lisberger, 2008; Yang and Lisberger, 2014). After trials where a complex spike occurred, reduced simple spike firing was found on the next trial; conversely, if no complex spike occurred, simple spike firing showed a slight increase on the next trial (Yang and Lisberger, 2014). Similar decreases in simple spike firing rate after a complex spike have been observed following saccades, with a less pronounced increase in simple spikes when no complex spike was present on the previous trial (Herzfeld et al., 2018).

The systematic movement errors that occurred in our adaptation condition might therefore be expected to result in reduced simple spike firing after the complex spike signal transmitted the error information, thereby reducing inhibitory tone (GABA) in the nuclei. Consistent with this, complex spike firing has been shown to serve as a teaching signal (Ma et al., 2016), leading to long-term depression (LTD) of parallel fiber-Purkinje cell synapses of those parallel fibers active simultaneously with the climbing fiber input (Marr, 1969; Albus, 1971; Ito and Kano, 1982). LTD in turn has been shown to result in decreased simple spike firing (Ito and Kano, 1982; Gao et al., 2003; Yang and Lisberger, 2014) and improve motor performance (Medina and Lisberger, 2008). Hence, it is plausible that a reduction in GABA concentration at the deep cerebellar nuclei could be tied to successful adaptation.

In line with the hypothesis that these adaption-related changes in GABA concentration are related to cerebellar plasticity, we demonstrated a correlation between the extent of early GABA changes in the right nuclei and adaptation. A greater decrease in GABA was related to better adaptation.

There are several potential explanations for the GABA increase in the contralateral nuclei during adaptation. One possible reason may be that the contralateral GABA increase may suppress output

from the side of the cerebellum that is nonrelevant to the adaptation task. Because the output would be relayed by the cerebellar nuclei, it is plausible that increased GABA in the contralateral cerebellar nuclei may serve to suppress output from the contralateral cerebellar hemisphere.

Simultaneous, but distinct, processes have been shown to underlie adaptation (Smith et al., 2006), including explicit and implicit processes (Taylor and Ivry, 2011; Taylor et al., 2014; McDougle et al., 2015; McDougle and Taylor, 2019), and the adaptation paradigm has been suggested to influence which processes are favored (Fleury et al., 2019). Indeed, there is evidence that implicit adaptation in visuomotor tasks is limited (Morehead et al., 2015, 2017), and it is possible that the adaptation paradigm used in this study led to the use of explicit strategies to counter the rotation. Further, although participants adapted substantially during the task, adaptation was incomplete as evidenced by the aftereffect. Both the recruitment of explicit strategies as well as the inability to fully adapt could potentially influence the physiological changes observed. Further research is required to determine the effect of different task paradigms on the differential recruitment of explicit and implicit processes and on enabling asymptotic adaptation, and future studies should explore how paradigm choice influences GABA changes observed in the cerebellum.

Cerebellar connectivity change is correlated with GABA in the nuclei

The adaptation-related GABA change in the right cerebellar nuclei was correlated with functional connectivity change in a cerebellar network so that a decrease in GABA was associated with stronger cerebellar network connectivity. This cerebellar network has previously been shown to increase in strength after adaptation, compared with after a control task (Albert et al., 2009; Nettekoven et al., 2020), in a performance-relevant manner (Nettekoven et al., 2020). We did not see a similar change here, perhaps because the resting-state scan in this study was not acquired immediately after the rotation blocks but after interspersed open loop blocks, which may have diluted a strength increase of the cerebellar network after adaptation.

Previous work from our lab and others has shown that GABA measured from a key node of a functional network is related to functional connectivity within that network (Kapogiannis et al., 2013; Stagg et al., 2014; Bachtiar et al., 2015). This finding therefore suggests that the relationship between local inhibition and connectivity may be a general property of functional networks, even in the context of the highly different physiology and anatomy of the cerebellar and cerebral cortices.

No GABA changes in the cerebellar cortex

In the cerebellar cortex, GABA is released by inhibitory interneurons in the molecular layer and the granule layer. Molecular layer interneurons, called basket and stellate cells, receive input from parallel fibers and inhibit Purkinje cells, resulting in disynaptic inhibition in parallel with the monosynaptic excitatory input from granule cells to Purkinje cells (Rieubland et al., 2014; Arlt and Häusser, 2020). In the granule layer, Golgi cells receive input from mossy fibers as well as granule cells and inhibit granule cells and other Golgi cells (Hull and Regehr, 2012). Although there is evidence that plasticity at molecular layer interneurons could regulate plasticity of parallel fiber–Purkinje cell synapses and influence adaptation *in vivo* (Rowan et al., 2018), there is no consensus yet on how precisely inhibitory interneurons in the cerebellar cortex contribute to adaptation learning.

We did not see significant changes in GABA in the cerebellar cortex during simple movement execution or during adaptation. It is possible that GABA concentration changes in the cerebellar cortex were not detectable with MRSI. It is also possible that the placement of the MRSI grid did not optimally cover or only incompletely covered the right-hand representation in the cerebellar cortex spanning right lobules 5 and 6 in the anterior cerebellum (Diedrichsen and Zotow, 2015). Future studies should probe the role of GABA in the cerebellar cortex directly by optimizing voxel size and placement so that potential changes in GABA in the right-hand representation in the cerebellar cortex are captured. Although not yet technically feasible, it would also be interesting to resolve changes at individual cerebellar nuclei and individual cerebellar lobules using finer MRSI resolution.

Conclusions

In this study, we present (to the best of our knowledge) the first investigation of cerebellar GABA changes during human visuomotor adaptation. We found movement-related GABA changes in the left and right cerebellar nuclei. When we controlled for these, we isolated GABA changes in the nuclei that were driven by adaptation. We found relationships between adaptation-driven GABA change in the right cerebellar nuclei and adaptation performance, and between adaptation-driven GABA change in the right cerebellar nuclei and change in cerebellar network connectivity. These results show the first evidence for plastic changes in cerebellar neurochemistry during a cerebellar learning task and provide the basis for developing therapeutic interventions that facilitate these naturally occurring changes to amplify cerebellar-dependent learning.

References

Albert NB, Robertson EM, Miall RC (2009) The resting human brain and motor learning. Curr Biol 19:1023–1027.

Albus JS (1971) A theory of cerebellar function. Math Biosci 10:25–61.

Alfaro-Almagro F, et al. (2018) Image processing and quality control for the first 10,000 brain imaging datasets from UK Biobank. Neuroimage 166: 400–424.

Andersson JLR, Jenkinson M, Smith S (2007) Non-linear registration aka spatial normalisation. FMRIB Technical Report TRO7JA2. Available at https://www.fmrib.ox.ac.uk/datasets/techrep/tr07ja2/tr07ja2.pdf.

Andersson JD, Matuskey D, Finnema SJ (2019) Positron emission tomography imaging of the γ-aminobutyric acid system. Neurosci Lett 691:35–43.

Arlt C, Häusser M (2020) Microcircuit rules governing impact of single interneurons on Purkinje cell output *in vivo*. Cell Rep 30:3020–3035.e3.

Bachtiar V, Near J, Johansen-Berg H, Stagg CJ (2015) Modulation of GABA and resting state functional connectivity by transcranial direct current stimulation. Elife 4:e08789.

Bates D, Mächler M, Bolker BM, Walker SC (2015) Fitting linear mixed-effects models using lme4. J Stat Softw 67:1–48.

Barmack NH, Yakhnitsa V (2013) Vestibulocerebellar connections. In: Handbook of the cerebellum and cerebellar disorders (Manto M, Schmahmann JD, Rossi F, Gruol DL, Koibuchi N, eds), pp 357–375. New York: Springer.

Bava A, Grimm RJ, Rushmer DS (1983) Fastigial unit activity during voluntary movement in primates. Brain Res 288:371–374.

Beckmann CF, Smith SM (2004) Probabilistic independent component analysis for functional magnetic resonance imaging. IEEE Trans Med Imaging 23:137–152.

Brooks JC, Faull OK, Pattinson KT, Jenkinson M (2013) Physiological noise in brainstem fMRI. Front Hum Neurosci 7:623.

Buckner RL, Krienen FM, Castellanos A, Diaz JC, Thomas Yeo BT (2011) The organization of the human cerebellum estimated by intrinsic functional connectivity. J Neurophysiol 106:2322–2345.

Cabanes E, Confort-Gouny S, Le Fur Y, Simond G, Cozzone PJ (2001) Optimization of residual water signal removal by HLSVD on simulated

short echo time proton MR spectra of the human brain. J Magn Reson 150:116–125.
Dean P, Porrill J, Ekerot CF, Jörntell H (2010) The cerebellar microcircuit as an adaptive filter: experimental and computational evidence. Nat Rev Neurosci 11:30–43.
Diedrichsen J (2006) A spatially unbiased atlas template of the human cerebellum. Neuroimage 33:127–138.
Diedrichsen J, Zotow E (2015) Surface-based display of volume-averaged cerebellar imaging data. PLoS One 10:e0133402–18.
Diedrichsen J, Hashambhoy Y, Rane T, Shadmehr R (2005) Neural correlates of reach errors. J Neurosci 25:9919–9931.
Diedrichsen J, Verstynen T, Schlerf J, Wiestler T (2010) Advances in functional imaging of the human cerebellum. Curr Opin Neurol 23:382–387.
Emir UE, Burns B, Chiew M, Jezzard P, Thomas MA (2017) Non-water-suppressed short-echo-time magnetic resonance spectroscopic imaging using a concentric ring k-space trajectory. NMR Biomed 30:e3714.
Emir UE, Sood J, Chiew M, Thomas MA, Lane SP (2021) High-resolution metabolic mapping of the cerebellum using 2D zoom magnetic resonance spectroscopic imaging. Magn Reson Med 85:2349–2358.
Fleury L, Prablanc C, Priot AE (2019) Do prism and other adaptation paradigms really measure the same processes? Cortex 119:480–496.
Floyer-Lea A, Wylezinska M, Kincses T, Matthews PM (2006) Rapid modulation of GABA concentration in human sensorimotor cortex during motor learning. J Neurophysiol 95:1639–1644.
Galea JM, Vazquez A, Pasricha N, Orban De Xivry JJ, Celnik P (2011) Dissociating the roles of the cerebellum and motor cortex during adaptive learning: the motor cortex retains what the cerebellum learns. Cereb Cortex 21:1761–1770.
Gao W, Dunbar RL, Chen G, Reinert KC, Oberdick J, Ebner TJ (2003) Optical imaging of long-term depression in the mouse cerebellar cortex *in vivo*. J Neurosci 23:1859–1866.
Gilbert PF, Thach WT (1977) Purkinje cell activity during motor learning. Brain Res 128:309–328.
Graydon FX, Friston KJ, Thomas CG, Brooks VB, Menon RS (2005) Learning-related fMRI activation associated with a rotational visuomotor transformation. Cogn Brain Res 22:373–383.
Griffanti L, Salimi-Khorshidi G, Beckmann CF, Auerbach EJ, Douaud G, Sexton CE, Zsoldos E, Ebmeier KP, Filippini N, Mackay CE, Moeller S, Xu J, Yacoub E, Baselli G, Ugurbil K, Miller KL, Smith SM (2014) ICA-based artefact removal and accelerated fMRI acquisition for improved resting state network imaging. Neuroimage 95:232–247.
Hardwick RM, Rottschy C, Miall RC, Eickhoff SB (2013) A quantitative meta-analysis and review of motor learning in the human brain. Neuroimage 67:283–297.
He Q, Duguid I, Clark B, Panzanelli P, Patel B, Thomas P, Fritschy JM, Smart TG (2015) Interneuron- and GABA(A) receptor-specific inhibitory synaptic plasticity in cerebellar Purkinje cells. Nat Commun 6:7364.
Herzfeld DJ, Kojima Y, Soetedjo R, Shadmehr R (2018) Encoding of error and learning to correct that error by the Purkinje cells of the cerebellum. Nat Neurosci 21:736–743.
Hull C, Regehr WG (2012) Identification of an inhibitory circuit that regulates cerebellar Golgi cell activity. Neuron 73:149–158.
Ichise T, Kano M, Hashimoto K, Yanagihara D, Nakao K, Shigemoto R, Katsuki M, Aiba A (2000) mGluR1 in cerebellar Purkinje cells essential for long-term depression, synapse elimination, and motor coordination. Science 288:1832–1835.
Ito M (2009) Cerebellar microcircuitry. In: Encyclopedia of neuroscience (Binder MD, Hirokawa N, Windhorst U, eds), pp 723–728. Berlin: Springer.
Ito M, Kano M (1982) Long-lasting depression of parallel fibre-Purkinje cell transmission induced by conjunctive stimulation of parallel fibres and climbing fibres in the cerebellar cortex. Neurosci Lett 33:253–258.
Jenkinson M, Smith S (2001) A global optimisation method for robust affine registration of brain images. Med Image Anal 5:143–156.
Jenkinson M, Bannister P, Brady M, Smith S (2002) Improved optimization for the robust and accurate linear registration and motion correction of brain images. Neuroimage 17: 825–841.
Jenkinson M, Beckmann CF, Behrens TEJ, Woolrich MW, Smith SM (2012) Review FSL. Neuroimage 62:782–790.
Jenkinson N, Miall RC (2010) Disruption of saccadic adaptation with repetitive transcranial magnetic stimulation of the posterior cerebellum in humans. Cerebellum 9:548–555.
Kapogiannis D, Reiter DA, Willette AA, Mattson MP (2013) Posteromedial cortex glutamate and GABA predict intrinsic functional connectivity of the default mode network. Neuroimage 64:112–119.
Klose U (1990) In vivo proton spectroscopy in presence of eddy currents. Magn Reson Med 14:26–30.
Kolasinski J, Hinson EL, Divanbeighi Zand AP, Rizov A, Emir UE, Stagg CJ (2019) The dynamics of cortical GABA in human motor learning. J Physiol 597:271–282.
Licata F, Occhipinti G, Santangelo F (1985) Responses of cerebellar fastigial neurons to single muscle activation. Exp Brain Res 60:127–135.
Ma Y, Shaik MA, Kozberg MG, Kim SH, Portes JP, Timerman D, Hillman EM (2016) Resting-state hemodynamics are spatiotemporally coupled to synchronized and symmetric neural activity in excitatory neurons. Proc Natl Acad Sci USA 113:E8463–E8471.
Marr JE (1969) A theory of cerebellar cortex. J Physiol 202:437–470.
Martin TA, Keating JG, Goodkin HP, Bastian AJ, Thach WT (1996) Throwing while looking through prisms. I. Focal olivocerebellar lesions impair adaptation. Brain 119 (Pt 4):1183–1198.
Medina JF, Lisberger SG (2008) Links from complex spikes to local plasticity and motor learning in the cerebellum of awake-behaving monkeys. Nat Neurosci 11:1185–1192.
McDougle SD, Bond KM, Taylor JA (2015) Explicit and implicit processes constitute the fast and slow processes of sensorimotor learning. J Neurosci 35:9568–9579.
McDougle SD, Taylor JA (2019) Dissociable cognitive strategies for sensorimotor learning. Nat. Commun 10:40.
Miall RC, Jenkinson EW (2005) Functional imaging of changes in cerebellar activity related to learning during a novel eye-hand tracking task. Exp Brain Res 166:170–183.
Moeller S, Yacoub E, Olman CA, Auerbach E, Strupp J, Harel N, Uğurbil K (2010) Multiband multislice GE-EPI at 7 tesla, with 16-fold acceleration using partial parallel imaging with application to high spatial and temporal whole-brain FMRI. Magn Reson Med 63:1144–1153.
Mottolese C, Richard N, Harquel S, Szathmari A, Sirigu A, Desmurget M (2013) Mapping motor representations in the human cerebellum. Brain 136:330–342.
Morehead JR, Qasim SE, Crossley MJ, Ivry R (2015) Savings upon re-aiming in visuomotor adaptation. J Neurosci 35:14386–14396.
Morehead RJ, Taylor JA, Parvin DE, Ivry RB (2017) Characteristics of implicit sensorimotor adaptation revealed by task-irrelevant clamped feedback. J Cogn Neurosci 29:1061–1074.
Myers L, Sirois MJ (2006) Spearman correlation coefficients, differences between. In: Wiley StatsRef: Statistics Reference Online (Balakrishnan N, Colton T, Everitt B, Piegorsch W, Ruggeri F, Teugels JL, eds). Available at https://doi.org/10.1002/9781118445112.stat02802.
Nettekoven C, Brady S, Clarke WT, Emir U, Levenstein J, Petitet P, Panouilleres MTN, Bachtiar V, O'Shea J, Johansen-Berg H, Jenkinson N, Stagg CJ (2020) GABA relates to functional connectivity changes and retention in visuomotor adaptation. bioRxiv. doi: 10.1101/2020.12.22.423981.
Nickerson LD, Smith SM, Öngür D, and Beckmann CF (2017) Using dual regression to investigate network shape and amplitude in functional connectivity analyses. Front Neurosci 11:115–118.
Orts-Del'Immagine A, Pugh JR (2018) Activity-dependent plasticity of presynaptic GABAB receptors at parallel fibre synapses. Synapse 72:e22027–12.
Popa LS, Streng ML, Ebner TJ (2019) Purkinje Cell representations of behavior: diary of a busy neuron. Neuroscientist 25:241–257.
Provencher SW (2001) Automatic quantitation of localized *in vivo* 1H spectra with LCModel. NMR Biomed 14:260–264.
Rieubland S, Roth A, Häusser M (2014) Structured connectivity in cerebellar inhibitory networks. Neuron 81:913–929.
Rowan MJM, Bonnan A, Zhang K, Amat SB, Kikuchi C, Taniguchi H, Augustine GJ, Christie JM (2018) Graded control of climbing-fiber-mediated plasticity and learning by inhibition in the cerebellum. Neuron 99:999–1015.e6.
Salimi-Khorshidi G, Douaud G, Beckmann CF, Glasser MF, Griffanti L, Smith SM (2014) Automatic denoising of functional MRI data: combining independent component analysis and hierarchical fusion of classifiers. Neuroimage 90:449–468.
Schlerf J, Ivry RB, Diedrichsen J (2012) Encoding of sensory prediction errors in the human cerebellum. J Neurosci 32:4913–4922.

Seidler RD, Noll DC, Chintalapati P (2006) Bilateral basal ganglia activation associated with sensorimotor adaptation. Exp Brain Res 175:544–555.
Smith SM (2002) Fast robust automated brain extraction. Hum Brain Mapp 17:143–155.
Smith MA, Ghazizadeh A, Shadmehr R (2006) Interacting adaptive processes with different timescales underlie short-term motor learning. PLoS Biol 4:1035–1043.
Stagg CJ, Bachtiar V, Amadi U, Gudberg CA, Ilie AS, Sampaio-Baptista C, O'Shea J, Woolrich M, Smith SM, Filippini N, Near J, Johansen-Berg H (2014) Local GABA concentration is related to network-level resting functional connectivity. Elife 3:e01465.
Steel A, Chiew M, Jezzard P, Voets NL, Plaha P, Thomas MA, Stagg CJ, Emir UE (2018) Metabolite-cycled density-weighted concentric rings k-space trajectory (DW-CRT) enables high-resolution 1 H magnetic resonance spectroscopic imaging at 3-Tesla. Sci Rep 8:7792.
Taylor JA, Ivry RB (2011) Flexible cognitive strategies during motor learning. PLoS Comput Biol 7:e1001096.
Taylor JA, Klemfuss NM, Ivry RB (2010) An explicit strategy prevails when the cerebellum fails to compute movement errors. Cerebellum 9:580–586.
Taylor JA, Krakauer JW, Ivry RB (2014) Explicit and implicit contributions to learning in a sensorimotor adaptation task. J. Neurosci 34:3023–3032.
Thach WT (1967) Somatosensory receptive fields of single units in cat cerebellar cortex. J Neurophysiol 30:675–696.
Thier P, Dicke PW, Haas R, Barash S (2000) Encoding of movement time by populations of cerebellar Purkinje cells. Nature 405:72–76.
Tseng Y-W, Diedrichsen J, Krakauer JW, Shadmehr R, Bastian AJ (2007) Sensory prediction errors drive cerebellum-dependent adaptation of reaching. J Neurophysiol 98:54–62.
Walsh DO, Gmitro AF, Marcellin MW (2000) Adaptive reconstruction of phased array MR imagery. Magn Reson Med 43:682–690.
Yang Y, Lisberger SG (2014) Role of plasticity at different sites across the time course of cerebellar motor learning. J Neurosci 34:7077–7090.